Theoretical study of the magnetism of Mn-doped ZnO with and without defects

D. Iuşan, B. Sanyal, and O. Eriksson
Department of Physics, Uppsala University, Box 530, SE-75121 Uppsala, Sweden
(Received 31 August 2006; published 11 December 2006)

We calculate the exchange interaction parameters of a classical Heisenberg Hamiltonian for Mn-doped ZnO (Mn concentration between 5% and 20%) by an *ab initio* Korringa-Kohn-Rostoker coherent-potential-approximation method in the framework of density functional theory. A weak antiferromagnetic exchange interaction is observed in pure Mn-doped ZnO in the dilute limit with an increase in the strength of interactions with increasing concentration of Mn. In the presence of donor defects, such as oxygen vacancies and interstitial Zn, the interactions remain antiferromagnetic, whereas in case of acceptor defects like Zn vacancies and N substitution of O, ferromagnetic interactions are observed. Due to the short-ranged character of interactions and disorder effects, the Curie temperatures calculated from Monte Carlo simulations yield low values (~45 K). However, in a few combinations of Mn and defect concentrations, the calculated Curie temperature can be as high as 135 K. If clustering of Mn atoms on a zinc-blende lattice is taken into account, the Mn-Mn spin correlations within a cluster are found to persist up to 600 K. Finally, we have shown that a modified mean-field theory, which we refer to as the "average mean field" estimate, yields values of the ordering temperature that are in good agreement with Monte Carlo simulations.

DOI: 10.1103/PhysRevB.74.235208 PACS number(s): 75.50.Pp, 75.70.−i, 71.70.Gm

I. INTRODUCTION

Diluted magnetic semiconductors have a great potential in spintronic applications,[1] justifying the tremendous research effort made in this field during the last few years. Despite this fact very few conclusive results have been achieved so far, thus keeping this field still in its infancy. One of the primary goals is to develop a ferromagnetic semiconductor operational at room temperature. For the most-explored and well-characterized diluted magnetic semiconductor (DMS), Mn-doped GaAs, the Curie temperature could not be raised more than 170 K.[2] Also, a general feature of III–IV semiconductors is that the doping limit of Mn is quite low (around 10%) and there is little hope that these systems can be used for the practical technological applications in the future.

In II–IV semiconductors, transition metals can be doped in much higher concentrations—e.g,. 20% for Cr in ZnTe and 35% for Co in ZnO—and ferromagnetic order can be achieved.[3] This opens up a possibility for the fabrication of new materials with desired properties. But it is fair to say that until now, these particular systems, especially oxide DMS, are less well characterized and conflicting experimental results have been published concerning the occurrence of high-temperature ferromagnetism.

In particular, several contradictory results on the magnetic properties of Mn-doped ZnO have been reported: paramagnetic,[4,5] spin-glass,[6] ferromagnetic at low temperatures,[7] or even ferromagnetic at room temperature.[8,9] To mention a few of the experiments, Sharma *et al.*[8] reported room-temperature ferromagnetism of low-temperature processed Mn-doped ZnO. It was argued by Kundaliya *et al.*[10] that the intrinsic ferromagnetism claimed in the above paper might have originated from the formation of a secondary phase—e.g., $Zn_xMn_{2-x}O_{3-\delta}$[10]—which was destroyed by annealing at high temperatures.[11] Furthermore, high temperature is needed for the growth of (polycrystalline) samples in which Mn substitutionally replaces Zn.[12]

Coey *et al.*[3] have suggested that high Curie temperatures can be obtained if the impurity bands hybridize with the 3*d* bands of the transition metal at the Fermi level. Concerning electronic structure calculations based on local-spin-density or gradient-corrected approximations, there is a general consensus that the dominant exchange interactions are the antiferromagnetic ones among the Mn atoms.[13–15] From self-interaction-corrected local-spin-density total-energy calculations, Petit *et al.*[16] found that Mn remains in a 2+ charge state in pure ZnO whereas a Mn^{3+} ion is more favorable in *p*-type ZnO. This implies that additional holes are required to fulfill the Zener model proposed by Dietl *et al.*[17]

Very recently, it was shown[18,19] that magnetic percolation effects are important in establishing long-ranged ferromagnetic (FM) interactions in these diluted magnetic systems. It was evident that distant-neighbor interactions play a crucial role in determining the T_C. Curie temperatures calculated from a mean-field approximation (MFA) are overestimated and the importance of Monte Carlo simulation (MCS) for a reliable calculation of Curie temperatures was emphasized. Also, mean-field theory always predicts a finite transition temperature for any finite concentration of impurities, thereby failing to capture the presence of magnetic percolation in the system. From the above discussions, it is clear that a detailed investigation of electronic structure and magnetic interactions is necessary, taking into account the general features of DMS's. In this paper, we intend to study in detail the exchange interactions between Mn spins with and without the presence of several probable defects followed by the calculation of T_C by MCS. The paper is organized as follows: the computational details are presented in the next section, followed by the results on pure Mn-doped ZnO. In Sec. IV we show the effects of donor and acceptor defects. Finally, Curie temperatures calculated by MCS are presented and compared to a modified mean-field theory for calculating the ordering temperatures.

II. COMPUTATIONAL DETAILS

The electronic structure calculations were performed using a Green's function Korringa-Kohn-Rostoker (KKR) method within the so-called atomic sphere approximation (ASA).[20] For the exchange-correlation functional, both the local spin density approximation (LSDA) and the generalized gradient approximation[21] (GGA) were used along with an *spdf* basis. As we will show below, the electronic structure has minor changes while using the GGA or LSDA.

The chemical and magnetic disorder were treated within the coherent potential approximation (CPA). The CPA is a single-site approximation and therefore it neglects local environment effects and possible lattice relaxations, but it has a computational advantage over the time-consuming supercell calculations.

Although Mn-doped ZnO crystallizes in the wurtzite structure, we have for simplicity considered the zinc-blende structure. This is a reasonable approximation as the strength of the exchange interactions does not vary much between these two structures to cause significant differences in the calculated critical temperatures. This will be discussed in more detail in Sec. III A. The zinc-blende unit cell consists of one Zn (Mn), one O, and two empty spheres in the interstitial positions in order to fulfill the applicability of the ASA. We used equal Wigner-Seitz sphere radii for all the atoms of the Zn and O sublattices, as well as for the empty spheres.

For the simulation of a disordered local moment (DLM) state, we have used the CPA for the spin-disordered medium where 50% of the Mn spins point in one direction and the rest point in the opposite direction.

The Heisenberg pair-exchange parameters were calculated using the theory of Liechtenstein *et al.*,[22] where the exchange interaction between two spins is calculated using a classical Heisenberg Hamiltonian employing the magnetic force theorem. The formula for pair-exchange parameter reads

$$J_{ij} = \frac{1}{4\pi}\int^{E_F} dE \,\mathrm{Im}\,\mathrm{Tr}_L(\Delta_i T_\uparrow^{ij}\Delta_j T_\downarrow^{ji}), \tag{1}$$

where $\Delta_i = t_{i\uparrow}^{-1} - t_{i\downarrow}^{-1}$, t being the on-site scattering matrix. T is the scattering path operator which is related to the off-diagonal element of the Green's function. Tr_L is the trace over the orbital indices of the scattering matrices. A positive (negative) J_{ij} represents ferromagnetic (antiferromagnetic) interactions. This methodology has been applied successfully to different magnetic systems in the past.[18,23,24] The use of the Heisenberg model is justified as the magnetic moments corresponding to the FM and DLM states do not differ by more than 1%, signifying the rigidity of spin in different environments.

The Curie temperatures were estimated both from the standard expression for the MFA and MCS using the calculated exchange parameters. The expression for the Curie temperature in the MFA of the Heisenberg model is

$$T_C^{MFA} = \frac{2x}{3k_B}\sum_{j\neq 0} J_{0j}, \tag{2}$$

where x is the concentration of Mn and k_B is the Boltzmann constant. We have also estimated Curie temperatures in the dilute limit using a modified form of Eq. (2). We will discuss this below along with a few examples.

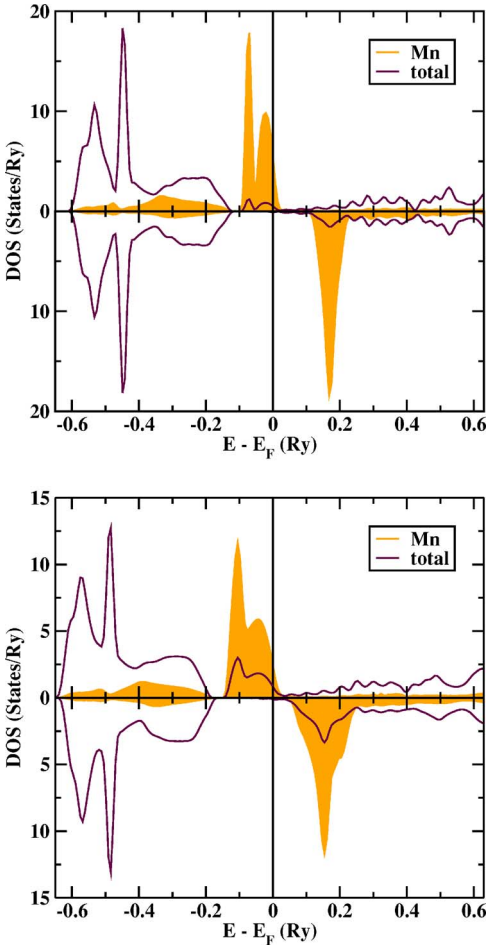

FIG. 1. (Color online) Calculated DOS of defect-free $Mn_{0.05}Zn_{0.95}O$ (upper panel) and $Mn_{0.20}Zn_{0.80}O$ (lower panel) in the FM state. The Mn states are shown in shade. Note that the Mn DOS and the total DOS are not shown on the same intensity scale.

The Monte Carlo simulations were done by the single-flip Metropolis algorithm. We have used simulation box sizes from $20\times20\times20$ to $80\times80\times80$. The critical temperatures were obtained from a fourth-order cumulant crossing method.[25] The fourth-order cumulant of the order parameter (magnetization) reads

$$U_L = 1 - \frac{\langle M^4\rangle}{3\langle M^2\rangle^2}. \tag{3}$$

From the intersection point of the curves of U_L for different system sizes L, we obtained the critical temperature.

III. RESULTS: PURE Mn-DOPED ZnO

We shall begin with an analysis of the electronic structure of defect-free $Mn_xZn_{1-x}O$ in the zinc-blende structure. This will serve mainly as a reference point and will allow us to point out later on the differences introduced by different defects.

In Fig. 1 we show the calculated density of states (DOS)

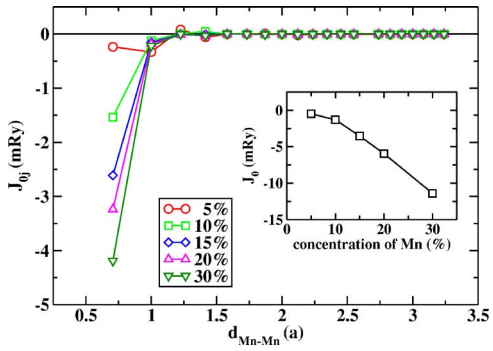

FIG. 2. (Color online) Calculated dependence of the exchange parameters on the distance between the magnetic atoms for various concentrations of Mn in $Mn_xZn_{1-x}O$. The inset presents the variation of the summed-up exchange interactions as a function of Mn content.

of defect-free $Mn_{0.05}Zn_{0.95}O$ in a ferromagnetic configuration (upper panel). In the lower panel the corresponding DOS of $Mn_{0.20}Zn_{0.80}O$ is shown. When Mn is doped in ZnO, it replaces a Zn atom to attain a 2+ charge state. This means that the electronic configuration of Mn remains almost in an atomic state, where the *d* states are half filled. The difference from a pure atomic configuration is that due to hybridization with ligand states (mainly O 2*p*), the width of the *d* level is finite and a rather strong hybridization tail is found in the entire region of oxygen states (from −0.6 to −0.1 Ry). The local environment of the Mn atoms in this structure gives rise to a crystal field splitting of the 3*d* states into the doubly degenerate *e* and triply degenerate t_2 states. The exchange splitting (~0.2 Ry) is much larger than the crystal field splitting; therefore, Mn is in a high-spin state (the Mn-projected moment is $\sim 4\mu_B$/atom). We would like to point out that our calculated band gap (~0.7 eV) is smaller than the experimental value of 3.4 eV.[26] As Fig. 1 also shows, the band gap increases with Mn content, as was also experimentally observed.[27,28] One may also note that the width of the *d* states increases with increasing Mn concentration, a result that is not unexpected.

The exchange interactions between the Mn atoms are shown in Fig. 2 as a function of Mn-Mn separation for different doping concentrations of Mn. The magnetic interactions are best characterized by a rather strong nearest-neighbor interaction that is antiferromagnetic (corresponding to negative values of J_{0j}). This interaction becomes stronger in magnitude with increasing Mn concentration (see inset of Fig. 2). Since this interaction seems not to be different from typical antiferromagnetic interactions in oxide materials, it is tempting to associate it with a superexchange mechanism.[29] The distant interactions are extremely weak and become exponentially damped with distance, as expected for magnetic interactions of magnetic elements in a semiconductor host.[30] Antiferromagnetic interactions between Mn ions in ZnO have actually been reported experimentally.[28,31,32] Although not shown here, there is a strong directional dependence of the *Jij*'s especially for small concentrations of Mn. This has been found also in other systems[33] and shows that it is difficult to use theoretical models which approximate the exchange interactions in dilute magnetic semiconductors with an isotropic parametrized form. One may also conclude from Fig. 2 that it is very unlikely that a substantial ordering temperature is to be expected in Mn-doped ZnO (without defects), at least in the concentration range below the percolation limit. If higher concentrations were to be realized, Fig. 2 suggests that the coupling is antiferromagnetic. We will return to this fact later in the paper.

We also investigated the difference between calculated magnetic moments and exchange interactions in the wurtzite and zinc-blende structures for $Mn_{0.05}Zn_{0.95}O$. The calculated magnetic moments differ by less than 5%. When comparing the exchange parameters for the nearest neighbors corresponding to the zinc-blende and wurtzite structures, one may observe some differences. For example, for 25% Mn doped in wurtzite ZnO the nearest-neighbor exchange is ~−2.5 mRy, while for 25% Mn in the zinc-blende structure the value is ~−3.5 mRy. In both structures the exchange interaction becomes very weak for longer-ranged interactions. Overall, $Mn_xZn_{1-x}O$ in the wurtzite structure has exchange interactions with a shape quite similar to the curves in Fig. 2 (which are for the zinc-blende structure).

Our calculated DOS for ZnO in the zinc-blende and wurtzite structures (data not shown) show minor differences. One noticeable difference is that the width of the Zn and O bands is somewhat smaller for the wurtzite structure; therefore, the hybridization is weaker for this structure.

IV. EFFECTS OF DEFECTS

Several defects or defect complexes can form during the growth of ZnO. Among these, the most common donor defects are oxygen vacancies (V_O) and zinc interstitials (Zn_I) leading to *n*-type ZnO. Other defects that could be encountered are zinc vacancies (V_{Zn}) and oxygen interstitials. Zinc vacancies and, also, oxygen substituted by nitrogen lead to a *p*-type material, which as we shall see in Secs. IV C and IV D has stronger ferromagnetic interactions compared to the pure Mn-doped ZnO system. Recent magnetization measurements of Mn-doped ZnO in the dilute limit[34] provide a clear indication of the enhancement of ferromagnetism by *p*-type doping and the opposite for *n*-type doping, and this is one of the motivations for studying defects theoretically. In addition, previous KKR-CPA calculations[35] of Mn-doped ZnO show that the ferromagnetism can be enhanced by *p*-type doping (with N), while the antiferromagnetic state becomes more stable by *n*-type doping. These conclusions were drawn from total-energy calculations by comparing the energies in the ferromagnetic and DLM states.

In the present analysis of defects we investigate the electronic structure, magnetic moments, and exchange interactions as a function of defect concentration. For those systems where dominating ferromagnetic interactions are found we have also used the interatomic exchange interactions in a Heisenberg Hamiltonian and calculated the critical temperature using Monte Carlo simulations. We have also compared these calculations with a modified mean-field expression for the ordering temperature (see Sec. IV E).

A. Zn interstitials

In the following we present the effect of Zn interstitials (Zn_I) on the electronic and magnetic interactions. The pro-

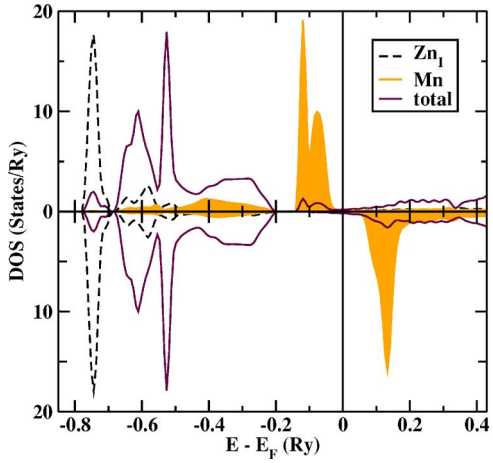

FIG. 3. (Color online) Calculated DOS of $Mn_{0.05}Zn_{0.95}O$ with 5% Zn_I incoporated. The Zn_I states are indicated by a dashed line, while the Mn states are shaded.

jected density of states in Fig. 3 indicates that Zn_I creates deep states about 0.07 Ry below the bottom of the valence band. As Zn_I's are added, the Fermi level moves up in energy and the Mn $3d\uparrow$ states become completely filled. Except for the appearance of the Zn_I states, the change in the electronic structure of Mn-doped ZnO can be approximated by a rigid-band model where the Fermi level simply is shifted up in energy as the concentration of Zn_I increases. Also, the energy shift between the O $2p$ and Mn $3d$ states increases by adding Zn_I, and this increases the energy gap. Finally we note that a small increase in the magnetic moment is found with increasing concentration of Zn_I, as shown in Fig. 4.

The calculated dependence of the exchange parameters between the Mn atoms as a function of distance and concentration of Zn interstitials (Fig. 5) reveals a dominant antiferromagnetic nearest-neighbor interaction. We find that the strength of the antiferromagnetic interactions can be very strong, of the order of 4–5 mRy. Our results are consistent with the calculations of Ref. 35 that point out that n-type doping leads to an increasing antiferromagnetic interactions.

B. Oxygen vacancies

Various theoretical and experimental papers concluded that oxygen vacancies are the predominant native defects act-

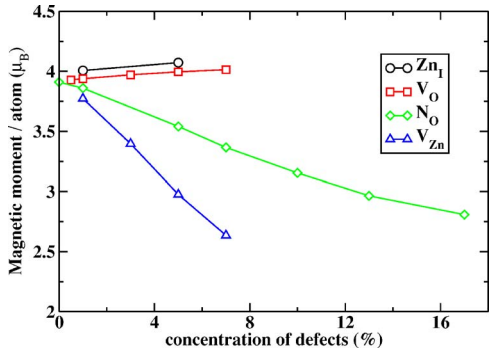

FIG. 4. (Color online) Calculated magnetic moments projected to the Mn atom for $Mn_{0.05}Zn_{0.95}O$ as a function of defect concentration.

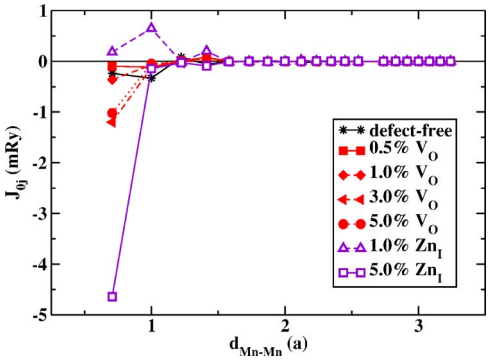

FIG. 5. (Color online) Calculated Heisenberg exchange parameters versus $d_{\text{Mn-Mn}}$ for various concentrations of Zn_I (open symbols) and V_O (solid symbols).

ing as donors in n-type ZnO. This has motivated us to consider their effect on the magnetic interactions in Mn-doped ZnO. Our calculations indicate that V_O actually has little effect on the electronic structure (data not shown) and the Mn-projected magnetic moment (Fig. 4). Also, in Fig. 5 we show the variation of the exchange parameters versus the Mn-Mn separation (for $Mn_{0.05}Zn_{0.95}O$) for different concentrations of oxygen vacancies. It is seen that the interactions among the Mn atoms are short ranged and rather small, ~ -1 mRy for the nearest-neighbor interaction. Depending on the defect concentration, the nearest-neighbor interaction can be ferromagnetic (1% Zn interstitials) or antiferromagnetic (5% Zn interstitials).

C. Zn vacancies

Among the native defects leading to p-type ZnO, zinc vacancies are thought to be the most predominant ones. Figure 6 presents the variation of the calculated exchange parameters of $Mn_{0.05}Zn_{0.95}O$ with the Mn-Mn distance for various concentrations of Zn vacancies.

It may be seen that p-type doping due to Zn vacancies (V_{Zn}) cause the interactions to become ferromagnetic. The interaction is again heavily dominated by a nearest-neighbor interaction. For some concentrations this exchange interaction becomes as high as 5.5 mRy, which must be considered

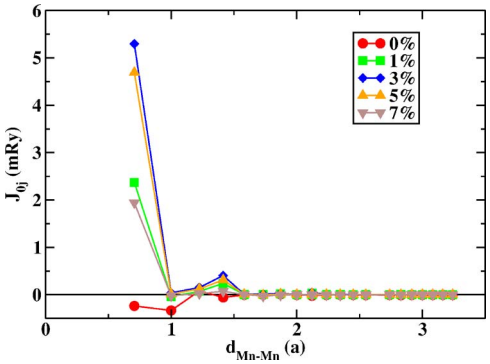

FIG. 6. (Color online) Calculated Heisenberg exchange parameters versus $d_{\text{Mn-Mn}}$ for various concentrations of Zn vacancies for the $Mn_{0.05}Zn_{0.95-x}O$ system.

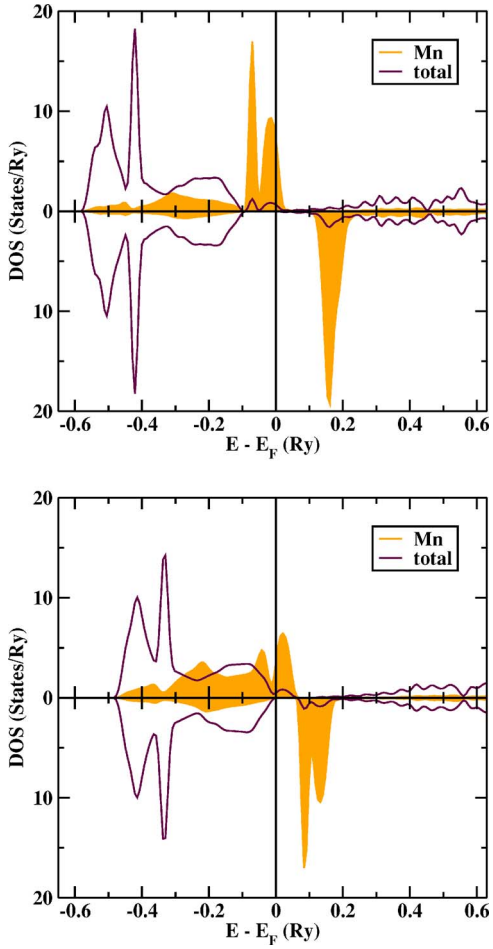

FIG. 7. (Color online) Calculated DOS of $Mn_{0.05}Zn_{0.95}O$ for a concentration of Zn vacancies of 1% (upper panel) and 7% (lower panel) for the $Mn_{0.05}Zn_{0.95-x}O$ system. The total DOS is indicated by a solid line, while the Mn states are scaled and shaded.

as a very strong ferromagnetic interaction. However, due to the strong nearest-neighbor interaction, a mean-field estimate of the ordering temperature yields a much more overestimated value[18] than the one obtained by Monte Carlo simulations (shown in Sec. IV E).

Figure 4 presents the variation of the magnetic moment with the concentration of Zn vacancies. The decrease of the Mn projected magnetic moment is much stronger than what is found for the other defects studied, and it is accompanied by a broadening of the Mn projected *d*-DOS (shown in Fig. 7). Figure 7 presents the DOS of $Mn_{0.05}Zn_{0.95}O$ for two different concentrations of Zn vacancies. It may be seen that with increasing amount of Zn vacancies the Mn *d* level moves down in energy, which causes a larger hybridization between the Mn *d* and ligand *p* orbitals. Hence the Mn levels broaden out to give a rather wide band, especially for a larger concentration of Zn vacancies (~5 eV for the spin up states). This is very important for the *p*-*d* exchange mechanism (discussed, e.g., in Ref. 36) and yields a strong ferromagnetic nearest-neighbor exchange.

The enhancement of ferromagnetism by Zn vacancies is confirmed also by total-energy calculations. Figure 8 presents the total energy of the Mn-doped ZnO system, without

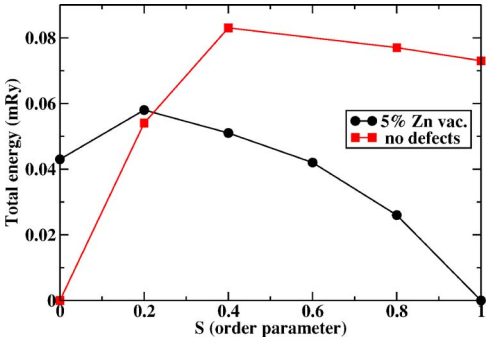

FIG. 8. (Color online) The variation of the total energy with the order parameter. The value $S=1$ corresponds to the FM state, while $S=0$ to the DLM state.

defects or with 5% V_{Zn}. The system is allowed to be either in a FM state, a DLM state, or a partially disordered local moment state. In the FM state, all Mn atoms have magnetic moments pointing in the same direction, corresponding to a value for the order parameter $S=1$. In the DLM state, half of the Mn atoms have magnetic moments pointing in one direction and the other half pointing in the opposite direction, corresponding to a value for the order parameter of $S=0$ (completely disordered magnetic state). In between the two liming cases, the FM and DLM ones, the partial DLM state is found, with $0<S<1$, for which part of the Mn atoms are pointing in one direction, while the rest is in the opposite direction. In case of pure Mn-doped ZnO, the minimum corresponds to the DLM state, while for 5% V_{Zn} the minimum corresponds to the magnetically ordered (FM) state ($S=1$). This indicates that the FM state is preferred over the DLM one in the presence of Zn vacancies, but the energy difference $E^{DLM}-E^{FM}$ is still rather small (~0.04 mRy).

D. Oxygen substitution by nitrogen

Having an electron less compared to O, N acts as an acceptor. As O is replaced by N, the number of electrons in the system decreases and the energy difference between ligand states and Mn *d* states becomes smaller. As a matter of fact, the N $2p$ states overlap in energy with the Mn $3d\uparrow$ states (Fig. 9), causing them to hybridize strongly. Hence one may expect that the interatomic exchange will, in a way similar to the Zn vacancies, become ferromagnetic when N is substituted for O. Wang *et al.*[37] have shown (from supercell calculations) that N enhances the ferromagnetism of Mn-doped ZnO ($Zn_{28}Mn_4O_{24}N_8$) and that Mn and N atoms prefer to exist as nearest neighbors. Our own results are in agreement with this finding. We show in Fig. 10 the exchange interaction between Mn atoms as a function of N concentration for $Mn_{0.05}Zn_{0.95}O_{1-x}N_x$. It may be noted that initially the nearest-neighbor interaction is increasing in magnitude as a function of N concentration and that a maximum is found at ~10% N, which after the exchange interaction decreases with increasing N concentration.

The variation of the magnetic moment with the concentration of N is showed in Fig. 4 and is found to decrease with increasing N concentration. This is due to the same mecha-

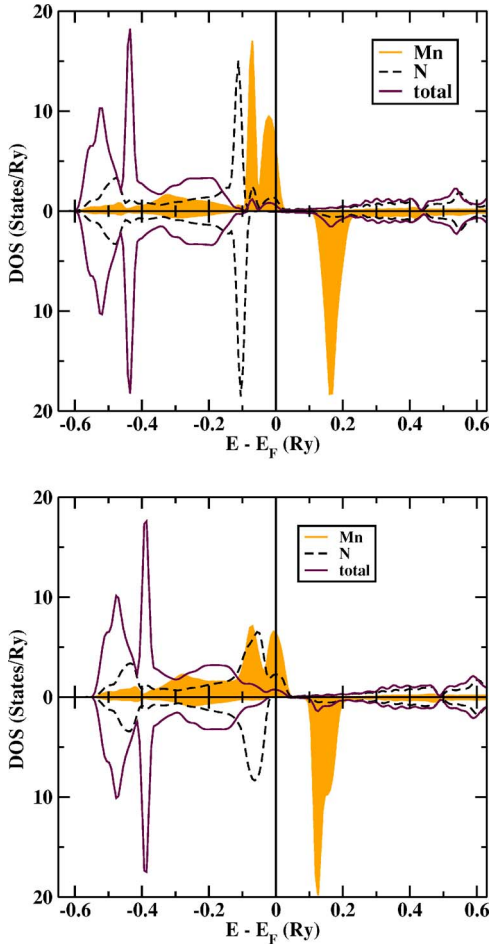

FIG. 9. (Color online) Calculated DOS of $Mn_{0.05}Zn_{0.95}O$ for a concentration of N substitution of 1% (upper panel) and 7% (lower panel) for $Mn_{0.05}Zn_{0.95}O_{1-x}N_x$. The Mn states are presented in shade, while the N states are indicated by a dashed line. Note that these states are scaled compared to the total DOS.

nism as discussed for the Zn vacancy defects, and it may be noted that the Mn-projected DOS are actually quite similar for the case of Zn vacancies and N defects.

We have also tested the stability of the ferromagnetic state versus the DLM state by total-energy calculations. For 5% N_O the ferromagnetic state was found to be lower in energy

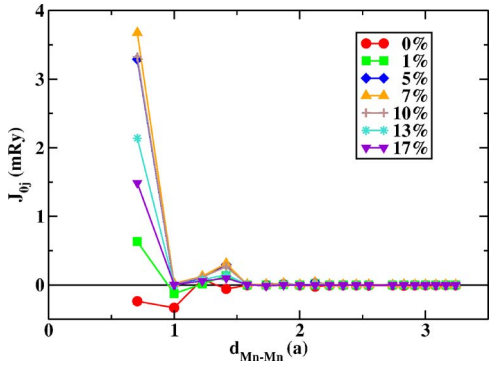

FIG. 10. (Color online) Heisenberg exchange parameters versus $d_{\text{Mn-Mn}}$ for various concentrations of N for $Mn_{0.05}Zn_{0.95}O_{1-x}N_x$.

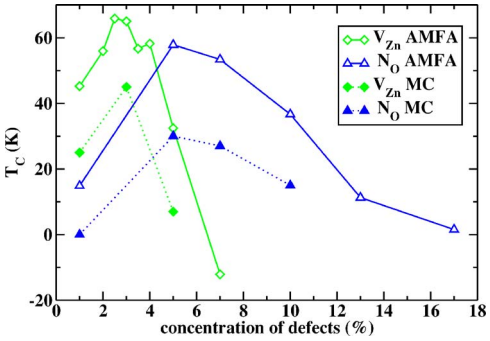

FIG. 11. (Color online) Curie temperatures calculated as a function of defect concentration by AMFA and MCS for two different types of defects for $Mn_{0.05}Zn_{0.95}O$-based systems.

with an energy difference $E^{\text{DLM}}-E^{\text{FM}}$ of approximately 0.08 mRy.

E. Ordering temperatures and an average mean-field approximation

For defects where ferromagnetic interactions are found—i.e., Zn vacancies and N substitution for O—we performed calculations of the Curie temperatures (for $Mn_{0.05}Zn_{0.95}O$) using a modified mean-field approximation. In this approximation, T_C was calculated by using the value of the exchange parameter corresponding to the average distance between Mn spins in the expression for mean-field solution of the Heisenberg model:

$$T_C^{AMFA} = \frac{2}{3k_B} J_{\langle 0j \rangle}, \tag{4}$$

where $\langle 0j \rangle$ corresponds to the *average* distance between the Mn atoms, which is determined by the concentration of Mn. A similar approach can be made to determine the exchange interactions by supercell calculations involving a large supercell with two magnetic atoms and calculating the total energies of ferromagnetic and antiferromagnetic alignments between them. The results of our calculations are shown in Fig. 11. As a comparison, we have also presented results from MCS. The average mean-field approximation (AMFA) curves are qualitatively similar to those calculated by MCS including the peak positions and the order of magnitude of the critical temperatures. It should be noted that the conventional mean-field expression [Eq. (2)] gives values of the ordering temperature that are one order of magnitude too large. However, it should also be noted that the method by Bouzerar *et al.*,[38] which treats spin fluctuations within a local random phase approximation, gives reliable results of the ordering temperature of Mn-doped GaAs and GaN. The quantitative difference is expected as MCS is an exact method. It is also seen that the calculation with Zn vacancies yields a Curie temperature between 10 and 50 K, with a maximum for ~3% defects. For the case when N is replacing O we find ordering temperatures reaching up to 30 K for a N concentration of 5%. Since 5% Mn is below the percolation limit for a nearest-neighbor model, it is not surprising that the calculated ordering temperatures are low.

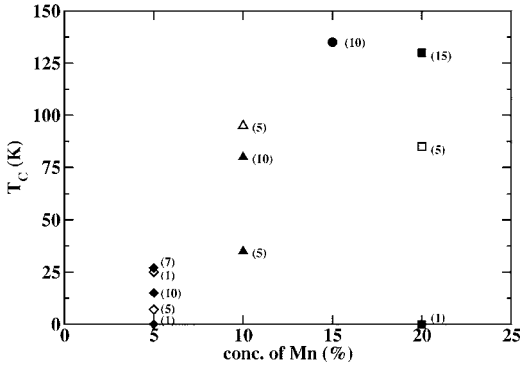

FIG. 12. Calculated Curie temperatures by Monte Carlo simulations. Solid symbols correspond to N substitution, while open symbols are for V_{Zn}. In the parentheses the concentration of defects is given.

In Fig. 12 we compile all our calculated values of T_C from the Monte Carlo simulations. The results for Zn vacancies and N-substituting O atoms are shown for various concentrations of these defects and Mn. A nonzero T_C indicates the existence of magnetic percolation in the presence of these defects. For a delicate balance of Mn and defect concentration, it is possible to obtain a T_C as high as 135 K—e.g., in case of 15% Mn- and 10% N-substituting O atoms. As shown in Fig. 2, the nearest-neighbor Mn-Mn interactions become more and more antiferromagnetic as the concentration of Mn is increased. However, this effect is counteracted in presence of acceptor defects and, as a result, a relatively high T_C is obtained.

Last, we want to comment on the high transition temperatures obtained in some experiments even for low Mn concentrations. We speculate that this is due to the presence of clusters containing a high concentration of Mn atoms. Inside these clusters, the Mn atoms are situated close to each other and a percolation path is established easily inside the cluster. As the nearest-neighbor Mn atoms have a strong antiferromagnetic coupling, the resulting transition temperature is expected to be very high. To test this hypothesis, we have calculated the exchange parameters for a zinc-blende MnO lattice. We have obtained a very large antiferromagnetic coupling between the nearest-neighbor Mn atoms. The calculated transition temperature from Monte Carlo simulations shows a very high value ($\sim$600 K), which is approximately the ordering temperature quoted in some experiments. This might suggest that these experiments showing high transition temperatures have inhomogeneities in the form of magnetic clusters, where the Mn concentration is very high. Since the cluster-cluster distances are very large, the magnetic coupling between them is expected to be vanishingly small. Hence, we suggest that these materials are best described as superparamagnetic.

V. CONCLUSION

We have investigated the electronic structure and magnetic interactions in Mn-doped ZnO in the presence and absence of a selection of defects. Our calculated Heisenberg exchange parameters show that in pure Mn-doped ZnO, the interactions between Mn spins are antiferromagnetic. This holds true also in the presence of certain defects—e.g., interstitial Zn and oxygen vacancies, where the defects are of donor type. In the case of *p*-type acceptor defects—e.g., Zn vacancy and nitrogen-substituting oxygen atoms–the interactions turn out to be ferromagnetic. Monte Carlo simulations yield small values of Curie temperatures ($<$50 K) for the case of acceptor defects and low Mn concentration. However, for a certain combination of defects, Curie temperatures can go up to 135 K. We have also compared a modified mean-field expression for the calculation of the ordering temperature to Monte Carlo simulations and found good agreement between the two. This suggests that it is possible to evaluate the ordering temperature from a supercell calculation with magnetic atoms at distances corresponding to the average distance appropriate for a given concentration. The energy difference between a ferromagnetic and antiferromagnetic configuration can then be used to estimate $J_{\langle 0j \rangle}$ in Eq. (4).

Finally, we comment on the applicability of the LSDA for the present system. Depending on the relative size of the electron-electron Coulomb repulsion—e.g., as given by the Hubbard U and bandwidth—one may expect that a theoretical method based on the LSDA might not be appropriate and that an LSDA+U,[39] Hubbard-I,[40] or dynamical mean-field theory[41] approach is more suitable. For the present study it is the Hubbard U of the Mn d states that should be compared to the bandwidth of these states, in order to asses the situation. Common estimates of the Hubbard U puts this value to range between 2 and 4 eV for Mn.[42] An inspection of Figs. 1, 7, and 9 shows that some of the cases studied here—e.g., 20% Mn in ZnO, 5% Mn in ZnO with Zn vacancies, or N substitution for O—give bandwidths of the order of 5 eV. For these systems the Hubbard U is smaller than the bandwidth and we expect an LSDA treatment to be reliable. However, for other concentrations of defects and/or varying Mn concentrations it is clear that the Mn d bandwidth approaches values of 1–2 eV, which suggests that a more direct inclusion of electron-electron interaction is appropriate. With this in mind it is not unlikely that a transition from localized to delocalized electron behavior (Mott transition) of the d states in these systems might occur as a function of defect concentration or as a function of Mn concentration. A systematic experimental study of this would clearly shine light on the nature of the electronic structure of these systems. However, as regards the interatomic exchange interactions it has been shown[18] that LSDA and LSDA+U give similar results, in that the general strength and range of the exchange interactions are the same from the two methods and that the calculated critical temperatures are similar. For this reason we do not expect that an LSDA+U calculation of the ordering temperatures of the presently studied system would deviate significantly from the values presented here.

ACKNOWLEDGMENTS

We are grateful to the Swedish Foundation for Strategic

Research (SSF), the Swedish Natural Science Research Council (NFR), and the Göran Gustafsson Foundation for financial support. We thank I. A. Abrikosov and A. Ruban for providing the KKR-CPA code for the calculation of exchange parameters. Lars Bergqvist is acknowledged for providing valuable suggestions regarding Monte Carlo simulations. Also, we acknowledge computational support from national resources provided by SNIC allocations.

[1] G. Prinz, Science **282**, 1660 (1998).
[2] T. Jungwirth, K. Y. Wang, J. Masek, K. W. Edmonds, J. König, J. Sinova, M. Polini, N. A. Goncharuk, A. H. MacDonald, M. Sawicki, R. P. Campion, L. X. Zhao, C. T. Foxon, and B. L. Gallagher, Phys. Rev. B **72**, 165204 (2005).
[3] J. M. D. Coey, M. Venkatesan, and C. B. Fitzgerald, Nat. Mater. **4**, 173 (2005).
[4] S. Kolesnik and B. Dabrowski, J. Appl. Phys. **96**, 5379 (2004).
[5] X. M. Cheng and C. L. Chien, J. Appl. Phys. **93**, 7876 (2003).
[6] T. Fukumura, Z. Jin, M. Kawasaki, T. Shono, T. Hasegawa, S. Koshihara, and H. Koinuma, Appl. Phys. Lett. **78**, 958 (2001).
[7] S. W. Jung, S.-J. An, G.-C. Yi, C. U. Jung, S.-I. Lee, and S. Cho, Appl. Phys. Lett. **80**, 4561 (2002).
[8] P. Sharma, A. Gupta, K. V. Rao, F. J. Owens, R. Sharma, R. Ahuja, J. M. Osorio Guillen, B. Johansson, and G. A. Gehring, Nat. Mater. **2**, 673 (2003).
[9] A. K. Pradhan, K. Zhang, S. Mohanty, J. B. Dadson, D. Hunter, J. Zhang, D. J. Sellmyer, U. N. Roy, Y. Cui, A. Burger, S. Mathews, B. Joseph, B. R. Sekhar, and B. K. Roul, Appl. Phys. Lett. **86**, 152511 (2005).
[10] D. C. Kundaliya, S. B. Ogale, S. E. Lofland, S. Dhar, C. J. Metting, S. R. Shinde, Z. Ma, B. Varughese, K. V. Ramanujachary, L. Salamanca-Riba, and T. Venkatesan, Nat. Mater. **3**, 709 (2004).
[11] J. Zhang, R. Skomski, and D. J. Sellmyer, J. Appl. Phys. **97**, 10D303 (2005).
[12] M. Kunisu, F. Oba, H. Ikeno, I. Tanaka, and T. Yamamoto, Appl. Phys. Lett. **86**, 121902 (2005).
[13] M. H. F. Sluiter, Y. Kawazoe, P. Sharma, A. Inoue, A. R. Raju, C. Rout, and U. V. Waghmare, Phys. Rev. Lett. **94**, 187204 (2005).
[14] L. M. Sandratskii and P. Bruno, Phys. Rev. B **73**, 045203 (2006).
[15] R. Janish, P. Gopal, and N. A. Spaldin, J. Phys.: Condens. Matter **17**, R657 (2005).
[16] L. Petit, T. C. Schulthess, A. Svane, Z. Szotek, W. M. Temmerman, and A. Janotti, Phys. Rev. B **73**, 045107 (2006).
[17] T. Dietl, H. Ohno, F. Matsukura, J. Cibert, and D. Ferrand, Science **287**, 1019 (2000).
[18] L. Bergqvist, O. Eriksson, J. Kudrnovsky, V. Drchal, P. Korzhavyi, and I. Turek, Phys. Rev. Lett. **93**, 137202 (2004).
[19] K. Sato, W. Schweika, P. H. Dederichs, and H. Katayama-Yoshida, Phys. Rev. B **70**, 201202(R) (2004).
[20] I. A. Abrikosov and H. L. Skriver, Phys. Rev. B **47**, 16532 (1993); A. V. Ruban and H. L. Skriver, Comput. Mater. Sci. **15**, 119 (1999).
[21] J. P. Perdew, K. Burke, and M. Ernzerhof, Phys. Rev. Lett. **77**, 3865 (1996).
[22] A. I. Liechtenstein, M. I. Katsnelson, V. P. Antropov, and V. A. Gubanov, J. Magn. Magn. Mater. **67**, 65 (1987).
[23] M. Pajda, J. Kudrnovský, I. Turek, V. Drchal, and P. Bruno, Phys. Rev. B **64**, 174402 (2001).
[24] J. Kudrnovský, I. Turek, V. Drchal, F. Máca, P. Weinberger, and P. Bruno, Phys. Rev. B **69**, 115208 (2004).
[25] D. P. Landau and K. Binder, *A Guide to Monte Carlo Simulations in Statistical Physics* (Cambridge University Press, Cambridge, England, 2000).
[26] *Numerical Data and Functional Relationships in Science and Technology*, Landolt-Börnstein, New Series, Vol. 196, edited by O. Madelung, M. Schulz, and H. Weiss (Springer-Verlag, Berlin, 1982), p. 35.
[27] A. Tiwari, C. Jin, A. Kvit, D. Kumar, J. F. Muth, and J. Narayan, Solid State Commun. **121**, 371 (2002).
[28] E. Chikoidze, Y. Dumont, F. Jomard, D. Ballutaud, P. Galtier, O. Gorochov, and D. Ferrand, J. Appl. Phys. **97**, 10D327 (2005).
[29] P. W. Anderson, Solid State Phys. **14**, 99 (1963).
[30] F. D. M. Haldane and P. W. Anderson, Phys. Rev. B **13**, 2553 (1976).
[31] S. W. Yoon, S.-B. Cho, S. C. We, S. Yoon, B. J. Suh, H. K. Song, and Y. J. Shin, J. Appl. Phys. **93**, 7879 (2003).
[32] E. Chikoidze, H. J. von Bardeleben, Y. Dumont, P. Galtier, and J. L. Cantin, J. Appl. Phys. **97**, 10D316 (2005).
[33] J. Kudrnovský, I. Turek, V. Drchal, F. Máca, P. Weinberger, and P. Bruno, Phys. Rev. B **69**, 115208 (2004).
[34] K. R. Kittilstved, N. S. Norberg, and D. R. Gamelin, Phys. Rev. Lett. **94**, 147209 (2005).
[35] K. Sato and H. Kamayama-Yoshida, Semicond. Sci. Technol. **17**, 367 (2002); Jpn. J. Appl. Phys., Part 2 **39**, L555 (2000); **40**, L334 (2001).
[36] P. H. Dederichs, K. Sato, and H. Katayama-Yoshida, Phase Transitions **78**, 851 (2005).
[37] Q. Wang, Q. Sun, P. Jena, and Y. Kawazoe, Phys. Rev. B **70**, 052408 (2004).
[38] G. Bouzerar, T. Ziman, and J. Kudrnovský, Europhys. Lett. **69**, 812 (2005).
[39] The first realistic implementation of a Hubbard U in a first-principles-based electronic structure method was made by F. Lopez-Aguilar and J. Costa-Quintana, Phys. Status Solidi B **123**, 219 (1984) and later followed by V. I. Anisimov, J. Zaanen, and O. K. Andersen, Phys. Rev. B **44**, 943 (1991).
[40] A. I. Liechtenstein and M. I. Katsnelson, Phys. Rev. B **57**, 6884 (1998).
[41] A. Georges, G. Kotliar, and M. J. Rosenberg, Rev. Mod. Phys. **68**, 13 (1996).
[42] G. Kotliar and D. Volhart, Phys. Today **57** (3), 53 (2004); L. Chioncel, M. I. Katsnelson, R. A. de Groot, and A. I. Liechtenstein, Phys. Rev. B **68**, 144425 (2003).